Solution Conformation of the Extracellular Domain of the Human Tumor Necrosis Factor Receptor Probed by Raman and UV-Resonance Raman Spectroscopy: Structural Effects of an Engineered PEG Linker†

Roman Tuma,‡ Malcolm Russell,‡ Mary Rosendahl,§ and George J. Thomas, Jr.*,‡

Division of Cell Biology and Biophysics, School of Biological Sciences, University of Missouri−Kansas City, Kansas City, Missouri 64110-2499, and Amgen Boulder, Inc., 3200 Walnut Street, Boulder, Colorado 80301

Received July 20, 1995; Revised Manuscript Received September 28, 1995⊗

ABSTRACT: The solution structure of the *Escherichia coli*-expressed extracellular domain, residues 12−172, of the human 55 kDa type I tumor necrosis factor receptor (TNFR) has been probed by Raman (514.5 nm) and ultraviolet-resonance Raman (244 nm) excitations. The Raman spectra have been collected from both the free TNFR domain and an engineered "dumbbell-like" derivative, consisting of two mutant receptor moieties linked by a 20 kDa polyethylene glycol (PEG) tether. The results demonstrate a TNFR secondary structure which is rich in β-sheet and deficient in α-helix, consistent with the reported X-ray crystal structure of baculovirus expressed receptor complexed with factor β [Banner, D. W., D'Arcy, A., Janes, W., Gentz, R., Schoenfeld, H.-J., Broger, C., Loetscher, H., & Lesslauer, W. (1993) *Cell 73*, 431-445]. Conversely, the solution structure of TNFR differs from the crystal structure in its distribution of disulfide rotamers and in the orientation of its unique indole side chain (tryptophan-107). These differences are attributed, respectively, to N-terminal truncation and factor binding in the TNFR crystal structure. The tryptophan configuration, which is easily monitored in both Raman and UVRR spectra, is proposed as a potential signal of receptor/factor recognition and binding. Application of the Raman probes to the engineered TNFR dumbbell, which is of interest as a potential therapeutic, shows that TNFR moieties of the dumbbell exhibit secondary structures and side chain environments which are indistinguishable from those of the native, wild-type moiety. The results suggest that the PEGylated dumbbell may function as an effective TNFR drug delivery system without the consequence of a deleterious antigenic response.

The tumor necrosis factor α (TNFα)[1] is a cytokine produced primarily by activated monocytes and macrophages in response to a physiological stress. TNFα has been identified specifically as a mediator of chronic autoimmune diseases, such as rheumatoid arthritis and multiple sclerosis, and as an agent in the pathology associated with sepsis. TNFα exists *in vivo* as a trimer of identical 17 kDa subunits and interacts with target cells via specific membrane receptors that act as transducing elements to trigger cellular responses. TNF receptors occur in virtually every mammalian tissue and cell group. There are two known receptor types (I and II) with apparent molecular masses of 55 and 75 kDa. Both receptors comprise four domains: a hydrophobic signal peptide; an intracellular domain; a transmembrane segment; and a soluble extracellular cysteine-rich domain which functions as the receptor locus.

The soluble extracellular domains of type I and type II receptors have been purified, sequenced, and cloned (Hale et al., 1995). They exhibit sequence homology (28%) (Dembic et al., 1990), and both are capable of binding either TNFα or TNFβ. Type I is thought to be the primary mediator of TNFα signal transduction (Tartaglia et al., 1993; Englemann et al., 1990). The recombinant type I gene encodes a single polypeptide chain of 161 amino acids, has a molecular mass 18.2 kDa, an isoelectric point of 6.9, and 24 cysteines forming 12 disulfides in the native conformation.

An *Escherichia coli* expressed TNF receptor domain (hereafter TNFR) has been crystallized, and its structure has been determined to 2.85 Å. (S. Sprang, personal communication). The overall folding pattern appears to be identical to that reported for the baculovirus derived type I domain complexed with TNFβ (Banner et al., 1993). On the basis of X-ray crystallographic data, TNFR is a member of the superfamily of receptor proteins which includes the extracellular domain of type II TNF receptor, CD40, Fas, and nerve growth factor receptor (Armitage, 1994). Proteins are assigned to this family on the basis of a repeating cysteine-rich sequence of 40 amino acids, typically containing three disulfide bridges. TNFR contains four such domains stacked end to end, forming a twisted linear rod.

Since cross-linking of two or more type I receptor molecules appears mandatory for the initiation of a cellular response, blocking of two of the three TNFα subunits should be sufficient for inactivation. Accordingly, we have designed a dimeric variant of TNFR for use as a potential therapeutic to sequester free TNFα during an inflammatory episode. Two

† Supported by NIH Grant GM50776.

* Author to whom correspondence may be addressed.
‡ University of Missouri−Kansas City.
§ Amgen Boulder, Inc.

⊗ Abstract published in *Advance ACS Abstracts,* November 1, 1995.

[1] Abbreviations: CD, circular dichroism; PEG, polyethylene glycol; PEGylation, linkage of two protein moieties by a PEG tether; TNF, human tumor necrosis factor; TNFR, soluble extracellular domain (residues 12−172) of the type I TNF receptor [sequence-numbering scheme of Banner et al. (1993)]; $TNFR^{N116C}$, TNFR containing the mutation of Asn-116 to Cys; $TNFR^{N116CC}$, $TNFR^{N116C}$ containing a cysteine residue disulfide-linked to Cys-116; $(TNFR^{N116C})_2PEG$, a dumbbell-shaped molecule consisting of two $TNFR^{N116CC}$ moieties PEGylated by a 20-kDa PEG linker; UVRR, ultraviolet-resonance Raman.

0006-2960/95/0434-15150$09.00/0

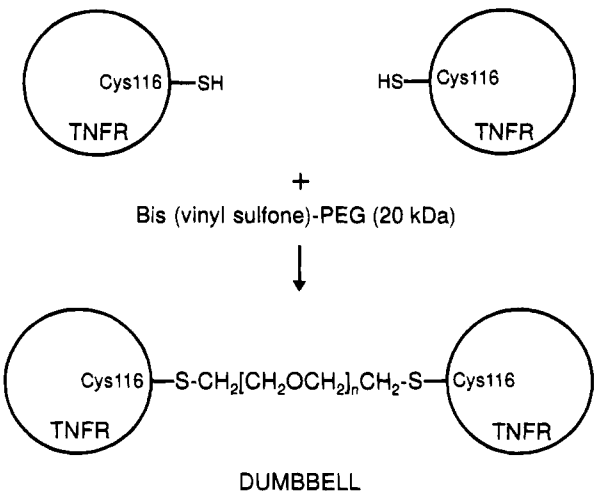

FIGURE 1: Cartoon representation of the TNFR dumbbell. Each mutant TNFR moiety ($TNFR^{N116C}$) is attached through a disulfide bridge at residue C116 to the 20-kDa PEG linker by reaction with the bis(vinyl sulfone) PEG reagent.

recombinant TNFR moieties, incorporating the mutation Asn-116 → Cys, are attached to one another in a dumbbell-like configuration at residue Cys-116 via a bifunctionally reactive 20 kDa polyethylene glycol (PEG) linker (Figure 1). We refer to the mutant as $TNFR^{N116C}$, to its disulfide-linked cystinyl derivative as $TNFR^{N116CC}$ and to the engineered dimer as $(TNFR^{N116C})_2PEG$. The dimer is expected to have enhanced potency for several reasons. First, the tethered TNFR moieties may exhibit enhanced avidity for the TNFα trimer as well as greater mobility in effecting a productive association. Dissociation of a $(TNFR^{N116C})_2PEG/TNF\alpha$ complex would require the unlikely event of simultaneous release of both TNFR moieties. Second, if $(TNFR^{N116C})_2$-PEG is able to bind two of the three TNFα subunits, then the remaining subunit may be unable to elicit the cellular response that requires clustering of receptors. Lastly, as with most "PEGylated" proteins, the larger molecular mass of $(TNFR^{N116C})_2PEG$ may result in an *in vivo* half-life greater than that of the monomer. Linkage of the two TNFR moieties by a flexible PEG tether is also expected to provide advantages of increased solubility and reduced rate of renal clearance (Abuchowski & Davis, 1981; Katre et al., 1987; Harris, 1992).

As noted above, the X-ray structure of *E. coli*-expressed TNFR appears to be identical to that of the baculovirus-expressed receptor (Banner et al., 1993). However, the PEGylated variant is not amenable to structure analysis by X-ray or NMR methods, owing to the presence of the PEG linker. Here, we demonstrate that off-resonance Raman spectroscopy and ultraviolet-resonance Raman (UVRR) spectroscopy provide valuable probes of the solution conformation and side chain environments of TNFR moieties in the $(TNFR^{N116C})_2PEG$ dumbbell. This investigation represents the first application of Raman and UVRR spectroscopy to a native protein which is so extraordinarily rich in cysteine (15% of residues). The data provide a framework for determining with high quantitative precision both the frequencies and intensities of specific Raman marker bands originating in the sulfur-containing side chains. We compare the structural information obtained from $(TNFR^{N116C})_2PEG$ with corresponding results obtained on the wild-type TNFR molecule and on the disulfide modified single-site mutant $TNFR^{N116CC}$. The Raman results on the TNFR solution structure are evaluated with respect to disulfide configurations reported recently for the crystal structure of baculovirus-derived TNFR (Banner et al., 1993). The implications of these results for *E. coli* expression and native folding of a eukaryotic protein and for use of PEGylation as a drug delivery strategy are discussed.

EXPERIMENTAL METHODS

1. Preparation and Purification of $TNFR^{N116C}$. *E. coli* cells containing the $TNFR^{N116C}$ expression plasmid were grown in a fermenter with medium containing phosphate, ammonium sulfate, citrate, and glycerol at 30 °C and pH 7.0. Sterilized trace minerals, magnesium sulfate, thiamine, and tetracycline were added before inoculation. The culture was induced by addition of IPTG when the OD_{660} was between 10 and 11. Fourteen hours after induction, the culture was harvested by centrifugation. The *E. coli* cells were isolated from 1000 L of fermentation broth and lysed by high-pressure homogenization.

The $TNFR^{N116C}$ inclusion bodies were recovered by centrifugation and solubilized in 8 M urea + 150 mM cysteine + 50 mM Tris at pH 9.5. After being stirred for 2 h at 20 °C, the reduced and denatured $TNFR^{N116C}$ was refolded by 20-fold dilution into 1.1 M urea + 50 mM Tris to yield a final refold solution composed of 250 μg of TNFR/mL, 1.5 M urea, 7.5 mM cysteine, and 50 mM Tris at pH 9.7. The resulting solution was stirred to allow for disulfide formation by air oxidation. The refold mixture was maintained at 6 °C for 2 days, brought to pH 5 by addition of HCl and acetic (Ac) acid, filtered to remove host proteins and misfolded TNFR, and loaded onto a 40 L column of S-Sepharose big bead resin equilibrated in 25 mM NaAc + 65 mM NaCl at pH 5.0 and 4 °C. After being loaded, the column was washed with the same equilibration buffer. $TNFR^{N116C}$ was eluted from the column using a salt gradient from 65 to 350 mM NaCl in 25 mM NaAc at pH 5.0 and 4 °C.

The S-Sepharose pool was diluted with 1.5 volumes of 5 M NaCl + 40 mM Na phosphate at pH 6 and loaded onto a 30 L Toyo Butyl 650 M column, previously equilibrated in 2.5 M NaCl + 20 mM Na phosphate at pH 6 and 20 °C. After being loaded, the column was washed with equilibration buffer and eluted with an inverse salt gradient from 2.5 to 1.0 M NaCl in 20 mM Na phosphate at pH 6.

The resulting pool was diafiltered against 5 volumes of 20 mM Na phosphate at pH 6 before being loaded onto a 30 L SP-Sepharose high-performance column equilibrated in 20 mM Na phosphate at pH 6 and 20 °C. After being loaded, the column was washed with equilibration buffer and eluted with a combination pH/salt gradient from 20 mM Na phosphate (pH 6) to 20 mM Na phosphate + 50 mM NaCl (pH 6.5).

The wild-type TNFR was prepared similarly to $TNFR^{N116C}$, except for a 25-fold reduction in scale.

2. Production of the $(TNFR^{N116C})_2PEG$ Dumbbell. $TNFR^{N116CC}$ was reduced to $TNFR^{N116C}$ with excess dithiothreitol (DTT). Free cysteine and unreacted DTT were removed by concentration/diafiltration (C/D) against 10 mM Na phosphate + 10 mM NaAc + 1 mM EDTA at pH 5. The pH of the C/D pool was adjusted to 7.5, and 20 kDa PEG bis(vinyl sulfone) reagent (Shearwater Polymers) was

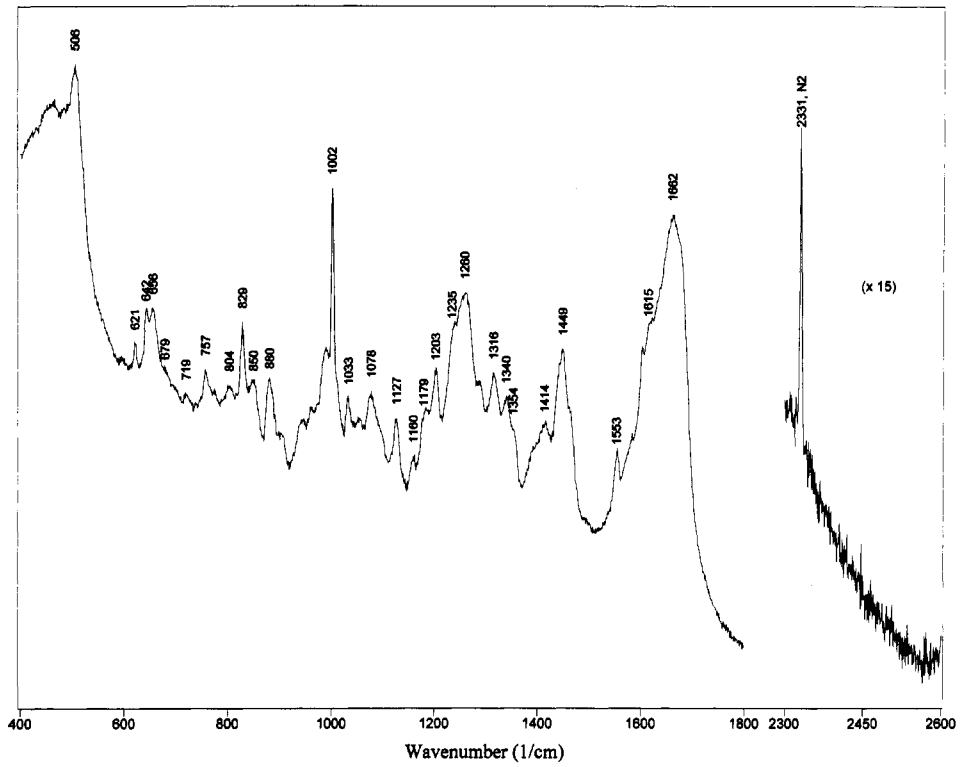

FIGURE 2: Raman spectrum (514.5 nm excitation) of the soluble extracellular domain of the human 55-kDa type I tumor necrosis factor receptor (residues 12−172; sequence: ^{12}DSVCPQGKY ^{21}IHPQNNSICC ^{31}TKCHKGTYLY ^{41}NDCPGPGQDT ^{51}DCRECESGSF ^{61}TASENHLRHC ^{71}LSCSKCRKEM ^{81}GQVEISSCTV ^{91}DRDTVCGCRK ^{101}NQYRHYWSEN ^{111}LFQCFCCSLC ^{121}LNGTVHLSCQ ^{131}EKQNTVCTCH ^{141}AGFFLRENEC ^{151}VSCSNCKKSL ^{161}ECTKLCLQPI ^{171}EN). The protein was dissolved to 153 mg/mL in H_2O at pH 7 and 10 °C. The spectrum is uncorrected for contributions from H_2O solvent in the region 400−1800 cm^{-1} and atmospheric N_2 in the region 2250−2650 cm^{-1} (amplified 15-fold). Raman frequencies of TNFR (labeled in cm^{-1} units) are assigned in Table 1 and discussed in the text.

added at a weight ratio of 0.5 g of PEG/g of protein. The mixture reacted for 15 h at 20 °C, yielding $(TNFR^{N116C})_2$-PEG, which was purified on a 14 L S-Sepharose high-performance column equilibrated in 50 mM Na phosphate at pH 3.1. $(TNFR^{N116C})_2$PEG was separated from unreacted and monosubstituted PEG using a NaCl gradient from 0.25 to 0.5 M in 50 mM Na phosphate at pH 3.1.

3. Spectroscopy. Visible excitation of off-resonance Raman spectra was accomplished with the argon 514.5 nm line from an Innova model 70 laser (Coherent, Inc., Santa Clara, CA) using 200 mW of radiant power at the sample. The spectra were collected at 6 cm^{-1} resolution on a model 1401 scanning spectrophotometer (SPEX Ind., Princeton, NJ). Samples were sealed in glass capillaries (Kimax #34507) and thermostated at 4 °C during scanning. Multiple scans of each sample were averaged in order to improve signal-to-noise ratios. Quantitative analysis of sulfhydryl concentrations was performed using the Raman band of gaseous N_2 (2331 cm^{-1}) as an external frequency and intensity standard (Tuma et al., 1993). Raman wavenumber calibration was performed with liquid indene.

The ultraviolet laser (Innova model 300 FRED, Coherent, Inc.), optical components, monochromator, and detector of the UVRR instrument have been described recently (Russell et al., 1995). The protein solution was maintained in a spinning quartz cell for presentation to the exciting radiation of wavelength 244 nm. UVRR spectra were collected with an effective spectral resolution of 5 cm^{-1}. Wavenumber calibration in UVRR spectra was performed using well-known Raman lines of dioxane, carbon tetrachloride, and acetonitrile.

The TNFR receptor is sensitive to prolonged exposure to 244 nm laser irradiation. Sample integrity was preserved by use of laser powers not exceeding 1 mW at the sample and by replacement of protein solutions in the spinning cell at 10 min intervals. Protein structural integrity was maintained at these conditions, as verified by established protocols (Russell et al., 1995).

RESULTS AND DISCUSSION

1. Raman Spectrum of TNFR and Assignments. Figure 2 shows the 514.5 nm-excited Raman spectrum of wild-type TNFR in the regions 400−1800 and 2250−2650 cm^{-1}. The Figure 2 spectrum, which is neither corrected for contributions of the aqueous buffer nor subjected to smoothing or other data refinement procedures, demonstrates the high quality of the experimental data. Evident in Figure 2 is the sharp Raman band of atmospheric N_2 at 2331 cm^{-1}, which serves as both a frequency and an intensity standard (Tuma et al., 1993). Prominent Raman bands of the protein are labeled in cm^{-1} units in Figure 2, and the proposed residue and subgroup vibrational assignments are listed in Table 1.

The extraordinarily intense Raman peak at 508 cm^{-1} and its shoulder at 522 cm^{-1} are assigned unambiguously to disulfide bond (S−S) stretching vibrations of cystine disulfides (Sugeta et al., 1973). The presence of this diagnostic band, as well as the absence of any detectable Raman SH band near 2550−2580 cm^{-1} (Figure 2), shows that all 24 Cys residues of wild-type TNFR are in the oxidized state. The same result is obtained for the 26 Cys residues (13 disulfides) of $TNFR^{N116CC}$. Further discussion of disulfide Raman markers of wild-type and mutant proteins is given

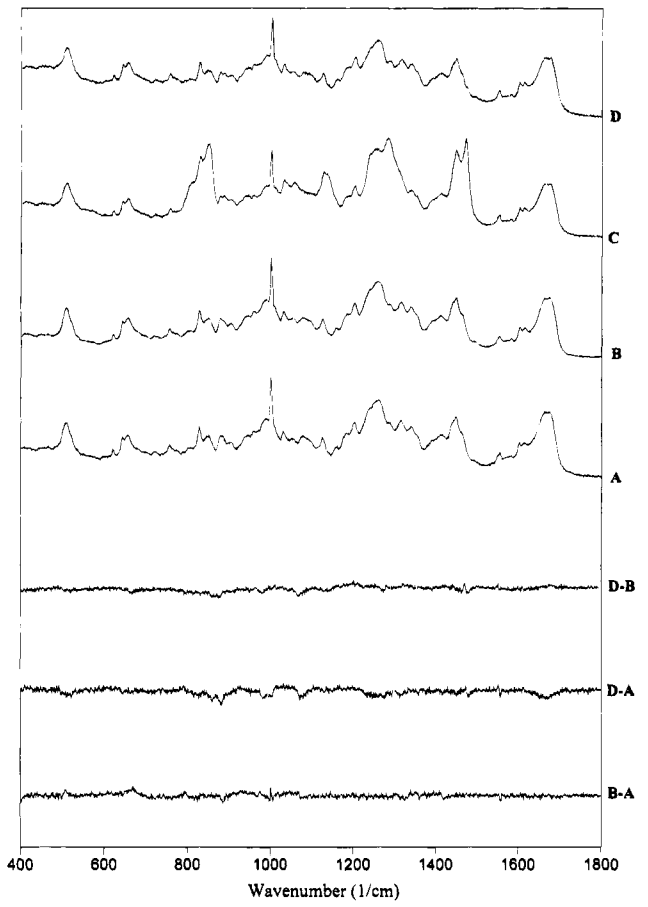

FIGURE 3: Upper panel: Raman spectra (514.5 nm) in the region 400−1800 cm^{-1} of aqueous solutions of wild-type TNFR (A), mutant $TNFR^{N116C}$ (B), bis-linked $(TNFR^{N116C})_2PEG$ (C), and bis-linked $(TNFR^{N116C})_2PEG$ which has been corrected for contributions of the PEG linker (D). Spectrum A is identical to that of Figure 2. Spectra B and C were recorded at conditions similar to those indicated in Figure 2. Spectrum D was obtained by subtraction of the solution spectrum of the PEG linker (not shown) from spectrum C. Lower panel: Computed difference spectra, B − A and D − A and D − B.

below in section 4.b.

2. Comparison of Raman Spectra of TNFR, $TNFR^{N116C}$, and $(TNFR^{N116C})_2PEG$. Raman spectra of the wild-type, mutant and bis-PEG-linked receptors, each excited at 514.5 nm, are shown in the upper panel of Figure 3. The computed difference spectra in the lower panel of Figure 3 provide a basis for identification of any primary, secondary and tertiary structural differences between the wild-type protein and its derivatized mutant (trace B − A), and between nonlinked and PEG-linked moieties (trace D − B). These are discussed below in sections 4.A and 4.C.

3. Comparison of Raman and UVRR Spectra of TNFR. Off-resonance (514.5 nm) and UVRR (244 nm) spectra of wild-type TNFR are compared in Figure 4. Using the resonance Raman excitation wavelength of 244 nm, the spectrum is dominated by bands of the five tyrosines (Y20, Y38, Y40, Y103, Y106) and single tryptophan (W107) of the receptor. Prominent bands in the off-resonance spectrum, which are too weak to be detected in the UVRR spectrum, are those of the five phenylalanines (F60, F112, F115, F143, F144), 24 half-cystines (C15, C29, C30, C33, C43, C52, C55, C70, C73, C76, C88, C96, C98, C114, C117, C120, C129, C137, C139, C150, C153, C156, C162, C166), numerous

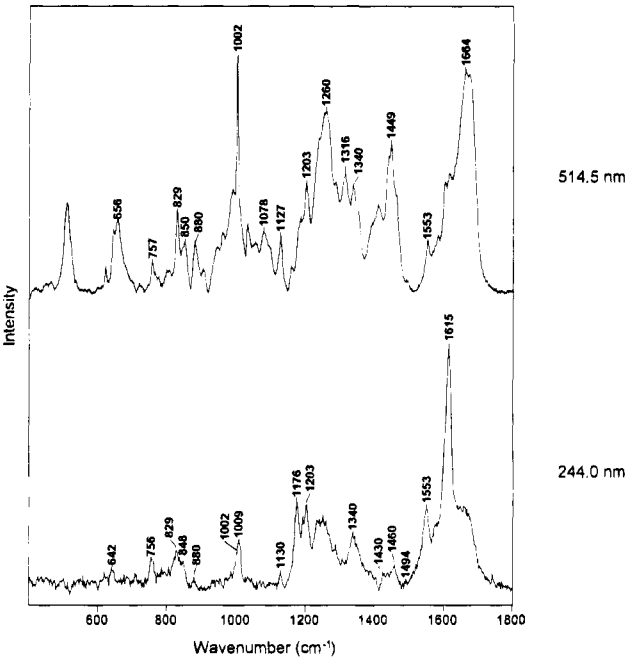

FIGURE 4: Comparison of off-resonance Raman (514.5 nm, top) and UVRR (244 nm, bottom) spectra of wild-type TNFR. The off-resonance spectrum is that of Figure 2, corrected for contributions of the aqueous buffer. The bottom spectrum was collected from a 5 mg/mL of solution of the protein at pH 7 and 20 °C, and is corrected for contributions of the aqueous buffer and quartz cell (Russell et al., 1995).

side chain aliphatic groups, and main chain amide groups. Specific assignments are given in Table 1.

4. Structural Interpretation. A. Main Chain Conformation. Raman frequencies of TNFR, which serve as indicators of main chain secondary structure, are identified at 1664 and 1677 cm^{-1} (amide I bands) and at 1239 and 1260 cm^{-1} (amide III bands). These markers are usually considered diagnostic of β-strand and irregular secondary structures (Thomas et al., 1987; Sargent et al., 1988), as indicated in Table 1. The absences of amide I intensity below 1655 cm^{-1} and amide III intensity above 1275 cm^{-1} are reliable indications of a deficiency of α-helix in the solution secondary structure of TNFR. The present Raman results, as well as CD spectra (unpublished data of M. Rosendahl) of the TNFR fragment 12−172, are consistent with the X-ray crystal structure of the related fragment 15−182 (Banner et al., 1993).

Although Raman spectra of TNFR do not permit a strict quantitative assessment of the solution secondary structure, the amide I spectral intensities at 1664 and 1677 cm^{-1} are consistent with comparable percentages of peptide groups in domains of β-strand and irregular conformations, the latter most likely including turns, loops, and disordered domains.

The presently observed invariance of Raman amide I and amide III bands to N116C mutation or bis-PEG linkage (Figure 3 difference spectra) shows further that these engineered changes in primary structure do not alter the solution secondary structure of the protein domain. Since band intensity changes as small as 2% are measurable by present methods (Prevelige et al., 1993), these results suggest that no more than three peptide groups per 161-residue TNFR moiety are altered in conformation (or hydrogen bonding) upon either N116C mutation or PEG tethering.

Table 1: Raman Frequencies and Assignments of the Human 55-kDa Tumor Necrosis Factor Receptor (Extracellular Domain, Residues 12−172)

Raman[a]	UVRR[b]	assignment[c]
506 (4.0)		Cys (S−S str, *ggg* conformer)
522 (2.2)		Cys (S−S str, *ggt* or *tgg* conformer)
621 (1.0)		Phe (*F6b*)
642 (2.5)	642 (0.7)	Tyr (*Y6b*)
656 (2.7)		Cys (C−S str)
678 (0.7)		Cys (C−S str)
720 (0.2)		Cys (C−S str)
757 (1.2)	756 (1.1)	Trp (*W18*)
809[d]		PEG (C−O−C sym str)
829 (3.6)	829 (1.5)	Tyr (*Y1* + *Y16a*)
850 (2.2)	848 (0.9)	Tyr (*Y1* + *Y16a*)
880 (2.2)	880 (0.4)	Trp (*W17*)
1002 (10.0)	1002 (1.4)	Phe (*F12*)
1010 (3.7)	1009 (1.9)	Trp (*W16*)
1030 (3.0)		Phe (*F18a*)
1040[d]		PEG (C−C str)
1062[d]		PEG (C−C str)
1127 (2.3)	1130 (0.6)	Trp (*W13*); aliph (CH_3 df)
1137[d]		PEG (C−O−C asym str)
1179 (2.7)	1176 (3.5)	Tyr (*Y9a*)
1203 (4.5)	1203 (3.4)	Tyr (*Y7a*)
1239 (6.6)	1235 (2.8)	amIII (β-strand)
1260 (7.7)		amIII (turns, loops); Tyr (*Y7a*)
1315 (5.3)		aliph (CH_2 df)
1341 (4.6)	1340 (2.1)	Trp (*W25* + *W33* or *W28* + *W29*)
1360 (2.8)	1360 (1.3)	Trp (*W25* + *W33* or *W28* + *W29*)
1415 (3.8)		Asp (CO_2^- str); Glu (CO_2^- str)
1449 (6.1)		aliph (CH_2 df)
1460 (4.0)	1460 (0.9)	aliph (CH_2 df); Trp (*W5*)
1553 (1.7)	1553 (3.3)	Trp (*W3*)
1601 (3.4)		Phe (*F8a*)
1615 (3.5)	1615 (10.0)	Tyr (*Y8a*)
1664 (7.8)		amI (β-strand, loops, turns)
1677 (7.8)		amI (turns, loops, β-strand)

[a] Raman frequencies (514.5 nm excitation) in cm^{-1} units and relative band intensities on an arbitrary 0−10 scale are from Figures 2−4 and additional spectra that are not shown. [b] UVRR frequencies (244 nm excitation) in cm^{-1} units and relative band intensities on an arbitrary 0−10 scale are from Figure 4 and additional spectra that are not shown. [c] Standard symbols are used for amino acids and functional groups; aliph indicates unspecified aliphatic side chains; italicized notation designates a specific normal vibrational mode (Austin et al., 1993) of the indicated side chain. Other abbreviations: am, amide, asym, asymmetric, str, stretching, sym, symmetric, df, deformation, sh, shoulder. Where more than one type of side chain or secondary structure contribute significantly to a Raman band, the major contributor is indicated first. [d] Raman bands due predominantly or exclusively to the PEG chain employed as a linker of mutant TNFR moieties. Identical bands are observed in the Raman spectrum of PEG (data not shown).

Amide I and amide III modes are also observed, though weakly, in the UVRR spectrum (Figure 4). Additionally, the UVRR spectrum provides evidence of a feeble amide II mode, observed as a low-frequency shoulder to the sharp tryptophan band at 1553 cm^{-1}. Both the frequency and intensity of the UVRR amide II mode are consistent with a deficiency of α-helical secondary structure in TNFR (Austin et al., 1993).

B. Side Chain Conformations and Interactions. (1) Cystine Disulfide Bridges. As noted above, cystine disulfide stretching vibrations of wild-type TNFR generate a very strong Raman band at 508 cm^{-1} with a weak shoulder at 522 cm^{-1} (Figure 2). The Raman frequency of a disulfide stretching mode is a sensitive indicator of the disulfide bridge configuration (Sugeta et al., 1973; Sugeta, 1975). Thus, the 508 cm^{-1} band identifies $C\alpha C\beta-S-S'-C\beta'C\alpha'$ disulfide bridges in which torsions about the $C\beta-S$ and $S'-C\beta'$ bonds are in the *gauche* range. (The *ggg* rotamer, for which the $S-S'$ torsion is also in the *gauche* range, is the most stable disulfide bridge configuration). On the other hand, the 522 cm^{-1} marker is diagnostic of a rotamer in which one carbon−sulfur torsion, either $C-S$ or $S'-C\beta'$, is in the *trans* range (i.e., *tgg* or *ggt*). The *tgt* rotamer, which is considered the least stable and which generates a characteristic Raman marker near 550 cm^{-1} (Sugeta et al., 1973), is not represented in the Raman spectrum of aqueous TNFR.

Relative intensities of the major 508 cm^{-1} band and its 522 cm^{-1} satellite may be estimated by either Fourier deconvolution or curve fitting of the experimental band profile, as shown in Figure 5. The results are consistent with 10 *ggg* rotamers, two *tgg* (or *ggt*) rotamers, and no *tgt* rotamers in the solution structure of TNFR.

In the X-ray crystal structure of the related TNFR fragment, 15−182, Banner and co-workers (1993) report coordinates for the 10 cystine bridges within the segment 15−149. Disulfide C15·C29 adopts the energetically unfavorable *tgt* conformation; disulfides C73·C88 and C117·C129 adopt the *ggt* conformation; and the remaining 7 disulfides adopt the most stable *ggg* conformation. (The two disulfides beyond residue 149 are not resolved in the X-ray structure, presumably due to local disorder in the crystal.) Since the Raman results demonstrate no *tgt* rotamer in fragment 12−172, we may conclude that one disulfide configuration differs between the solution and crystal structures. The likely candidate is C15·C29. Its conformational peculiarity (*tgt*) in the crystal can be rationalized as an N-terminal effect, possibly reflecting intermolecular forces in the crystal lattice which are absent in the solution environment. Truncation of three additional N-terminal residues in the fragment crystallized by Banner et al. may also be a contributing factor to stabilization of an otherwise energetically unfavorable *tgt* rotamer at this site.

The occurrence of all $S-S'$ torsions of the crystal structure within a typical *gauche* range (i.e., 75−105°) is consistent with the Raman solution structure.

The broad band centered at 656 cm^{-1} in Figure 2 is due primarily to carbon−sulfur stretching vibrations of cystine bridges exhibiting *gauche* $C-S$ torsions. [The very small contribution expected from a similar mode of the single methionine residue (M80) is not resolved in present spectra. The broad 656 cm^{-1} marker is also overlapped on its low-frequency side by two unrelated sharp bands, which represent characteristic modes of tyrosine (642 cm^{-1}, *Y6b*) and phenylalanine (620 cm^{-1}, *F6b*), as assigned in Table 1.] On the high-frequency side of the 656 cm^{-1} band we observe shoulders occurring near 678 and 720 cm^{-1}, assignable to $C-S$ stretching modes of *trans* $C-S$ rotamers. The low intensities of these shoulders in relation to the principal 656 cm^{-1} band confirm that $C\beta-S$ and $S'-C\beta'$ torsions in cystine bridges of the TNFR solution structure are overwhelmingly in the *g* conformation (Sugeta et al., 1973), consistent with the foregoing analysis of $S-S'$ stretching bands.

The difference spectrum B − A of Figure 3 shows that in the C116 mutant there are weak but significant Raman bands near 506 and 667 cm^{-1} which are not present in wild-type TNFR. These difference bands demonstrate that the engineered disulfide of $TNFR^{N116CC}$ exists in the *ggg* conformation.

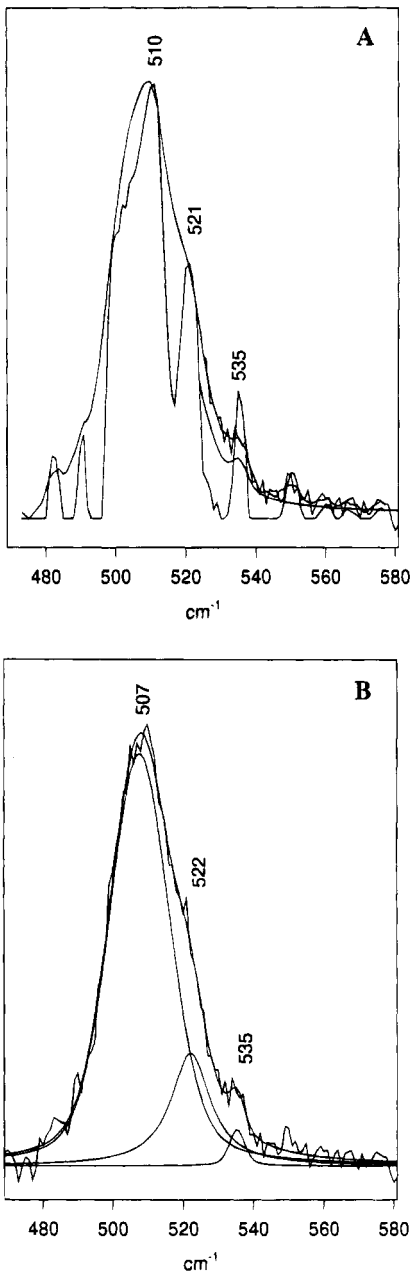

FIGURE 5: Decomposition of the cystine disulfide band profile in the region 480−560 cm^{-1} of the Raman spectrum of wild-type TNFR. (A) Fourier deconvolution using a Lorentz−Gauss desmearing function of 18 cm^{-1} half-width (Thomas & Agard, 1984) after smoothing of the raw data (Savitzky-Golay, 9 point average). The deconvolved components at 510 and 521 cm^{-1} are assigned respectively to the 506 and 522 cm^{-1} S−S stretching modes (Table 1), the feeble peak at 535 cm^{-1} to a non-cystinyl side chain vibration, probably tryptophan (Miura et al., 1989), and the much weaker satellites to deconvolution artifacts. (B) Curve fitting of the band profile to the minimum number of Lorentzian components. Data from Figure 2 were corrected for solvent background prior to decomposition procedures.

The difference spectrum D − A of Figure 3, by virtue of the absence of difference bands in the 500−700 cm^{-1} region, shows that disulfide configurations are invariant to PEG tethering of the protein moieties.

(2) Tyrosine Hydrogen Bonding. The five tyrosines of the wild-type TNFR exhibit a Fermi doublet at 854 and 832 cm^{-1}, for which the ratio of peak heights (I_{854}/I_{832}) is diagnostic of the hydrogen bonding states of phenoxyl donor and acceptor atoms (Siamwiza et al., 1975). The presently observed ratio, $I_{854}/I_{832} = 0.6$ (for both 514.5 and 244.0 nm excitations), indicates that all five phenoxyl OH groups act as hydrogen bond donors and that at least three of the five are likely donors of a very strong hydrogen bond to a highly electronegative acceptor. Among obvious acceptor candidates are the numerous aspartate (5) and glutamate (11) carboxyls which are interspersed throughout the TNFR sequence. (See Figure 2 caption.)

UV excitation (Figure 4) enhances the tyrosine modes *Y8a* (1615 cm^{-1}), *Y7a* (1203 cm^{-1}), and *Y9a* (1176 cm^{-1}). A relationship has been proposed between the frequency of *Y8a* and the strength of phenoxyl hydrogen bonding (Rodgers et al., 1992). Thus, *Y8a* at 1615 cm^{-1} is considered indicative of a strong hydrogen bond donor. Since the five tyrosines of the receptor contribute to the observed band, we may conclude that all phenoxyls are strong hydrogen bond donors, in accordance with the conclusion reached from the off-resonance Raman spectrum.

The present results show also that the phenoxyl hydrogen bonding characteristics of the receptor tyrosines are unaffected by the N116C mutation and bis-PEG derivatization.

(3) Indole Environment of Tryptophan-107. Both the off-resonance and resonance Raman spectra of TNFR are informative of the environment of its single tryptophan residue (W107). In Figures 2 and 4, the position of indole ring mode *W3* (1553 cm^{-1}) indicates that the magnitude of the torsion angle $|\chi^{2,1}|$ (Cβ−C3 bond torsion) is approximately 100°, which is approximately 20° lower than observed in the crystal structure. Since the tryptophan ring in the crystal is located on a surface proximal to bound TNF, it is likely that the local conformation in the crystal is affected by substrate binding.

The frequency of mode *W17* (880 cm^{-1}) indicates moderate hydrogen bonding of the indole N1H donor. Additionally, both Raman (Figure 2) and resonance Raman (Figure 4) intensities for the Fermi doublet components at 1340 and 1360 cm^{-1} (measured as the ratio of peak intensities, I_{1360}/I_{1340}) are indicative of a hydrophilic environment for the indole ring of residue W107 (Miura et al., 1989).

Raman bands of W107 evident in the UVRR spectrum but absent from the off-resonance spectrum are assigned to *W6* (1430 cm^{-1}), *W4* (1494 cm^{-1}), and *W2* (1579 cm^{-1}). Although each UVRR band is weak, its position confirms moderate hydrogen bonding for the indole N1H donor (Miura et al., 1989), in accordance with the off-resonance spectrum.

The W107 environment, N1H interaction, and side chain torsion are all unaffected by the N116C mutation and bis-PEG derivatization.

C. Effect of the PEG Linker upon the Structure of the TNFR Fragment. Spectrum C of Figure 3 serves to identify the principal Raman bands characteristic of the PEG linker. These occur within the interval 810−850 cm^{-1} (assigned to symmetrical stretching of C−O−C bonds), and at 1040 and 1062 cm^{-1} (C−C stretching), 1137 cm^{-1} (C−O−C asymmetric stretching), and 1245, 1283, and 1450−1472 cm^{-1} (various CH_2 deformations). Raman assignments for the linker are catalogued in Table 1. After correction of spectrum C of Figure 3 for PEG linker contributions, we obtain the spectrum D of Figure 3. Comparison of D with native unlinked TNFR generates the virtually null difference spectrum, D − B of Figure 3. This demonstrates that the PEG linker has no significant effects upon secondary

structure or side chain environments of TNFR moieties to which it is tethered.

SUMMARY AND CONCLUSIONS

We have employed Raman and UV-resonance Raman probes to examine the solution structure of the *E. coli*-expressed extracellular domain (residues 12−172) of the 55 kDa type I human tumor necrosis factor receptor. We find that the solution secondary structure of this TNFR moiety is rich in β-sheet and irregular domains but deficient in α-helix, consistent with the tertiary folds observed in X-ray crystal structures of the same sequence expressed in *E. coli* (S. Sprang, personal communication) and a closely similar sequence expressed in baculovirus (residues 15−169 complexed with TNFβ) (Banner et al., 1993). However, we find that the distribution of disulfide bridge geometries in the solution structure differs significantly from that in the published crystal structure, presumably due to effects of N-terminal truncation and/or packing in the crystal. The solution TNFR structure lacks the *tgt* disulfide rotamer proposed for disulfide C15:C29 in the crystal.

Remarkably, the single tryptophan residue (W107) of TNFR exhibits a significantly different side chain torsion in the solution structure ($|\chi^{2,1}| \approx 100°$) than in the crystal structure (120°). Since the W107 indole ring is proximal to bound TNFβ in the crystal, the difference may reflect a specific interaction at the factor/receptor interface. We propose that the unique tryptophan residue of TNFR undergoes a change of indole orientation in response to binding of factor. Thus, the tryptophan residue may function as a signal of receptor recognition and binding.

Raman probes were also employed to compare the solution conformations and side chain environments of wild-type, mutant, and tethered TNFR moieties. The native fold of the TNFR extracellular domain is invariant to the N116C mutation and to tethering two moieties by a 20 kDa PEG linker. Likewise, the numerous side chains monitored by the Raman spectrum, including the 12 intramolecular disulfide bridges and many aromatic and aliphatic residues, are unaffected by N116C mutation and PEGylation.

Several PEGylated proteins are presently being evaluated in clinical trials, including PEG-asparaginase for treatment of acute leukemias, PEG-adenosine deaminase for severe combined immunodeficiency disease, and PEG-superoxide dismutase and PEG−catalase for reducing tissue injury associated with ischemia. As with any peptide-related human pharmaceutical, strict attention must be given to maintaining the native conformation in order to minimize antigenic response. In the case of TNFR, this is particularly important since antibodies against TNFR have the potential to cross-link cell surface receptors and elicit a TNF-like cytotoxic response. The present results indicate that PEGylation can be effected without significant perturbation of the native protein conformation and may represent a generally effective means for drug delivery without adverse antigenic response.

ACKNOWLEDGMENT

We thank Dr. Claire Careaga for suggesting the collaboration that led to this research.

REFERENCES

Abuchowski, A., & Davis, F. F. (1981) in *Enzymes as Drugs* (Holsenberg, J., & Roberts, J., Eds.) pp 367−383, Wiley, New York.

Armitage, R. J (1994) *Curr. Opin. Immunol. 6*, 407−413.

Austin, J., Jordan, T., & Spiro, T. G. (1993) in *Advances in Spectroscopy* (Clark, R. J. H., & Hester, R. E., Eds.) Vol. 20, pp 55−127, Wiley, London.

Banner, D. W., D'Arcy, A., Janes, W., Gentz, R., Schoenfeld, H.-J., Broger, C., Loetscher, H., & Lesslauer, W. (1993) *Cell 73*, 431−445.

Dembic, Z., Loetscher, H., Gubler, H., Pan, Y.-C. E., Lahn, H.-W., Gentz, R., Brockhaus, M., & Lesslauer, W. (1990) *Cytokine 2*, 231−237.

Engelmann, H., Holtmann, H., Brakebusch, C. Avni, Y. S., Sarov, I., Nophar, Y., Hadas, E., Leitner, O., & Wallach, D. (1990) *J. Biol. Chem. 265*, 14497−14504.

Hale, K. K., Smith, C. G., Baker, S. L., Vanderslice, R. W., Squires, C. H., Gleason, T. M., Tucker, K. K., Kohno, T., & Russell, D. A. (1995) *Cytokine 7*, 26−38.

Harris, J. M., Ed. (1992) *Poly(ethylene glycol) Chemistry: Biotechnical and Biomedical Applications*, Plenum Press, New York.

Katre, N. V., Knauf, M. J., & Laird, W. J. (1987) *Proc. Natl. Acad. Sci. U.S.A. 84*, 1487−1491.

Miura, T., Takeuchi, H., & Harada, I. (1989) *J. Raman Spectrosc. 20*, 667−671.

Prevelige, P. E., Thomas, D. H., Aubrey, K. L., Towse, S. A., & Thomas, G. J., Jr. (1993) *Biochemistry 31*, 537−543.

Rodgers, K. R., Su, C., Subramaniam, S., & Spiro, T. G. (1992) *J. Am. Chem. Soc. 114*, 3697−3704.

Russell, M., Vohnik, S., & Thomas, G. J., Jr. (1995) *Biophys. J. 68*, 1607−1612.

Sargent, D., Benevides, J. M., Yu, M.-H., King, J., & Thomas, G. J., Jr. (1988) *J. Mol. Biol. 199*, 491−502.

Siamwiza, M. N., Lord, R. C., Chen, M. C., Takamatsu, T., Harada, I., Matsuura, H., & Shimanouchi, T. (1975) *Biochemistry 14*, 4870−4876.

Sugeta, H. (1975) *Spectrochim. Acta 31A*, 1729−1737.

Sugeta, H., Go, A., & Miyazawa, T. (1973) *Bull. Chem. Soc. Jpn. 46*, 3407−3411.

Tartaglia, L. A., Ayres, T. M., Wong, G. H. W., & Goedell, D. V. (1993) *Cell 74*, 845−853.

Thomas, G. J., Jr., & Agard, D. A. (1984) *Biophys. J. 46*, 763−768.

Thomas, G. J., Jr., Prescott, B., & Urry, D. W. (1987) *Biopolymers 26*, 921−934.

Tuma, R., Vohnik, S., Li, H., & Thomas, G. J., Jr. (1993) *Biophys. J. 65*, 1066−1072.

BI951675V